JOURNAL OF MATERIALS SCIENCE 31 (1996) 4433–4442

Microstructures and metastable phases produced in cold sintered blocks by mechanical alloying of NiAl–TiB_2

TIANYI CHENG
Metal Materials Section, Dept. No. 7, Beijing Institute of Technology, P.O. Box 327, Beijing 100081, P.R. China; and International Centre for Materials Physics, Academia Sinica, Shengyang 110015, P.R. China

The microstructure of cold sintered blocks formed on the mechanical alloying (MA) of NiAl–TiB_2 have been investigated by means of transmission electron microscopy (TEM). The results reveal that the blocks consisted of β-NiAl with a B2 ordered structure and TiB_2, Al_2O_3 particles in addition to other metastable phases. The distribution of the phases and good bonding between them suggest that a sintering process occurred *in-situ* at low temperature in the later stage of the MA. The observed high density of dislocations and strong reaction between these dislocations and ceramic particles can explain the good toughness and high microhardness of the block. Minor crystalline and amorphous metastable phases have been found. A cold-sintering mechanism to form the block based on the metastable phase distribution has been proposed.

1. Introduction

Mechanical alloying together with an appropriate consolidation process is an attractive approach to producing composites with high strength values at elevated temperatures and reasonable toughness behaviour at room temperature. This is due to fine microstructures and homogeneously distributed reinforcements, including inherently produced oxide dispersoids. The process has been successfully applied in recent years to fabricate intermetallic NiAl-based composites [1–4], which exhibit improved mechanical properties.

MA is a powder processing technique that requires the high-energy ball milling of the elemental powders and thus involves extensive collision, grinding and friction between the powders and balls. This results in considerable pulverisation and deformation of the initial powders, which significantly promotes the solid state diffusion in a very small scale. Due to the very high mechanical energy involved and the normally long running time, MA is a far-from equilibrium process. Hence, MA not only produces nanometer sized microstructures, but can create unique disordered structures [5] and novel phases [6], these can include amorphous phases and supersaturate solid solutions. Consequently, MA is not only an effective approach to producing advanced materials but also an efficient way to study the formation of special microstructures and metastable phase transformations in the solid state. It has found particular use in the study of intermetallics with high negative formation enthalpy. These have included a metastable disordered phase and an amorphous phase in MA Ni_3Al [5, 6], metastable NiAl and an amorphous phase in MA nickel-rich Ni_xAl_{100-x} ($65 < x < 73$) [7] and the metastable supersaturate solid solution, intermetallic phase ($\varkappa$) and amorphous phase in MA NiAlTi [8]. However, no metastable phase has been reported in MA stoichiometric or near-stoichiometric NiAl or NiAl-based composites probably due to the very large negative formation enthalpy (about -59– $-72\ kJ\ mol^{-1}$ [9]) and the high structural stability of the ordered B2 structured β-NiAl.

It is evident that an understanding of the mechanism creating the formation of microstructures and metastable phases in MA materials and hence controlling the MA process are important if we wish to tailor the microstructures and mechanical properties of the final consolidated materials. Unfortunately, progress in this area has been limited [6] due to difficulties in monitoring the process.

We have reported [10] on the production of a special cold sintered block with a macroscopic size (up to several centimeters), and homogeneous composition (Ni–30.9 wt % Al–4.5 wt % TiB_2) by MA Ni–34 wt % Al–3 wt % TiB_2 (designated NiAl–TiB_2) powders. Its structure was investigated by means of x-ray diffraction (XRD) and scanning electron microscopy (SEM). As a continuation of the previous work, the microstructures and metastable phases in the cold sintered block have been further studied using transmission electron microscopy (TEM) and a possible mechanism for the formation of the cold sintered block has been developed.

0022–2461

2. Experimental Procedures

The detailed information relating the MA process of the elemental powders and of NiAl–TiB_2 is reported elsewhere [10]. The microstructures of the cold sintered block were studied by means of a Jeol-2000FX TEM at 200 kV. The microcompositional analysis was performed using the energy dispersive spectroscopy (EDS) facility in the TEM. Specimens for the TEM were prepared by cutting slices of 0.2 mm thickness from the cold sintered blocks by means of an electric spark cutting machine. The slices were further thinned by grinding on SiC papers to about 60 μm thickness. The 3-mm-diameter disks were then again cut using an electric spark machine. The disks were dimpled on both sides using a dimple grinder and subsequently ion milled under a voltage of 5 kV. One dimpled disk was further thinned by a two-jet electropolisher in a solution of 10 vol % sulphuric acid and 90 vol % methanol. No important difference in the microstructures between the foils prepared by ion milling and electropolishing was found.

3. Results and discussion

3.1. Microstructure

3.1.1. Phases and grain structures

The cold sintered block consisted mainly of a matrix of β-NiAl with a B2 ordered structure (Fig. 1). The EDS and selected area electron diffraction (SAED) analyses show that the small particles on the grain boundaries of β-NiAl are TiB_2 and Al_2O_3 (Fig. 1a) created by the pulverisation of the oxide film of the elemental aluminium powders. Many very fine TiB_2 particles are also distributed within the grains (Fig. 1c, Fig. 3(a, b)). In addition to the metastable phases (see Section 3.2) no pure nickel or pure aluminium was found. These findings are basically consistent with the results of XRD and SEM examinations [10] although no peaks from Al_2O_3 and the metastable phases were found in the XRD patterns of the block. This is probably due to their small concentrations compared to the detection limit of XRD. Moreover, the bonding between the ceramic particles and the matrix is good and no obvious pores or evidence for melting was observed, thus suggesting that the block is dense on the microscale investigated by TEM. The average grain size is about 2 μm and is close to that observed by means of SEM (5.6 μm). Many tweed-like striations along some directions can be seen in some grains of the β-NiAl (Fig. 1c) but no obvious corresponding streaks are present in the SAED pattern. These sort of striations were not observed in a hot pressed MA NiAl–TiB_2–Y_2O_3 (Ni–33.1 wt % Al–2 wt % TiB_2–0.5 wt % Y_2O_3) composite [11], which has a similar composition to the present NiAl–TiB_2 composite and was also prepared by MA processing before consolidation. Hence, the striation may be associated with defects created in MA powders that are retained in the block.

The SEM examination revealed that some grains in the cold sintered block exhibit unique curved grain boundaries [10]. This was confirmed by TEM investigation. The three grains in Fig. 2a connect to each other in a triple-junction and all have curved grain boundaries so that a small independent triangular area was formed in the junction. The SAED and EDS analyse show that the three grains all are nickel-rich β-NiAl (Table I) with some heavy striations. The small concentration of iron in the β-NiAl grains probably resulted from the stainless steel balls used in the MA. According to the SAED patterns and calculations the curved grain boundaries are not coherent boundaries and the angle between any two grains is not small (14°, 18° and 26° respectively). It is probable that the grain boundary with a curved appearance has a lower energy than that of a normal grain boundary. The kinetic reasons for the formation of this unique grain boundary will be further investigated.

TABLE I The Composition (at %) of the three grains around a triple-junction

	Ni	Al	Fe
Grain I	53.5	45.9	0.6
Grain II	56.9	42.5	0.6
Grain III	54.6	45.0	0.4

3.1.2. Dislocation structure

The dislocation density in most grains of the cold sintered block is very high (Fig. 3(a, b)), suggesting that the high density of defects produced in MA of the powders by extensive deformation did not significantly decrease in the block after the cold snitering. Dislocation generation from the interface between the matrix and the ceramic particles and the grain boundaries was also observed (Fig. 1a), this behaviour is similar to that found in a consolidated MA NiAl–TiB_2–Y_2O_3 composite [11]. Considering the very limited dislocation density found in normal β-NiAl [12] and the temperature rise during MA, the high density of dislocations in the cold sintered block implies that the block experienced extensive plastic deformation after its formation by cold sintering. This also suggests that the block has good toughness and ductility, which was partly confirmed by observations of microhardness indents [10]. The detailed SAED analysis indicates that the dislocation configuration in β-NiAl is the normal $\{1\,1\,0\}\langle 0\,0\,1\rangle$ type and no new type of dislocations were identified. Moreover, it can be seen from Fig. 3(a, b) there are many dislocation loops in the block. A high concentration of supersaturated vacancies, up to about 10^{-6} has been reported for MA powders with a grain size of 10–30 nm [13] although the vacancy concentration in normal copper at 300 K is only about 10^{-12} [14]. Most of the vacancies may be retained in the cold sintered block and the collapse of these vacancies leads to the formation of dislocation loops [15]. In addition, there is a strong reaction between dislocations and the very fine TiB_2 particles (Fig. 3a). The dislocations were pinned by the TiB_2 particles in many places and show Orowan bowing, which can explain why the block has high microhardness (443 kg mm^{-2} [10]). Some dislocation loops surrounding the particles locate just behind the bowing dislocation, suggesting that

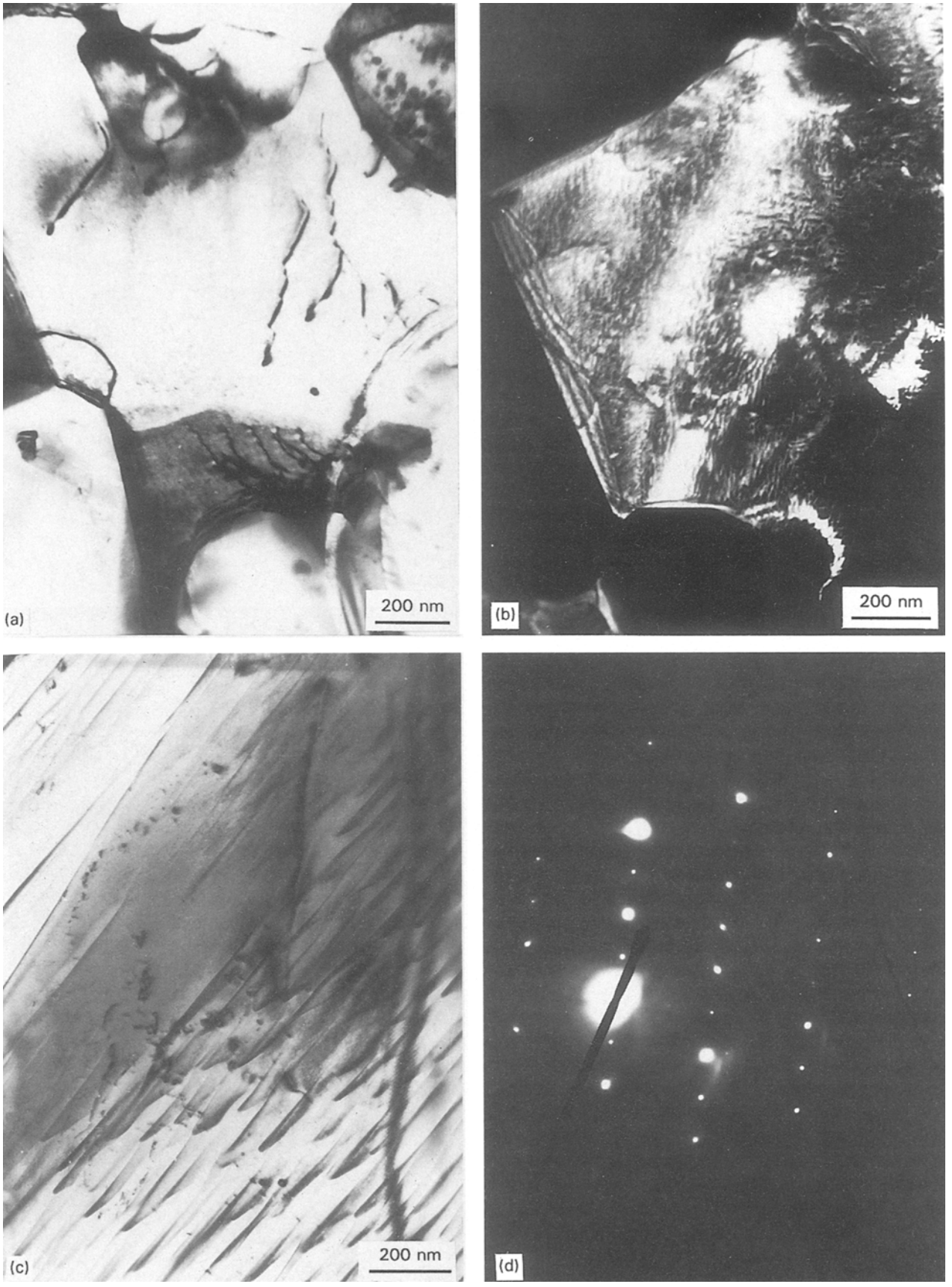

Figure 1 Microstructures of the cold sintered block (a) β-NiAl matrix and TiB_2 (T), Al_2O_3 (A) particles, (b) dark field of β-NiAl grain ($g = 1\,\bar{1}\,0$), (c) striations in some β-NiAl grains (d) SAED pattern of β-NiAl, B2 [0 1 2] zone.

the dislocation loop was left after the dislocation past over the particles in the plastic deformation during MA. The size difference amongst the loops is quite large and some big loops with a zig-zag curvature are present, implying that the loop growth occurred when the loop met other vacancies after it had formed. The low angle subgrain boundaries consisting of a dislocation array are also present in some grains (Fig. 3(c, d)). Many grains in the block show a polygon-like appearance when examined by

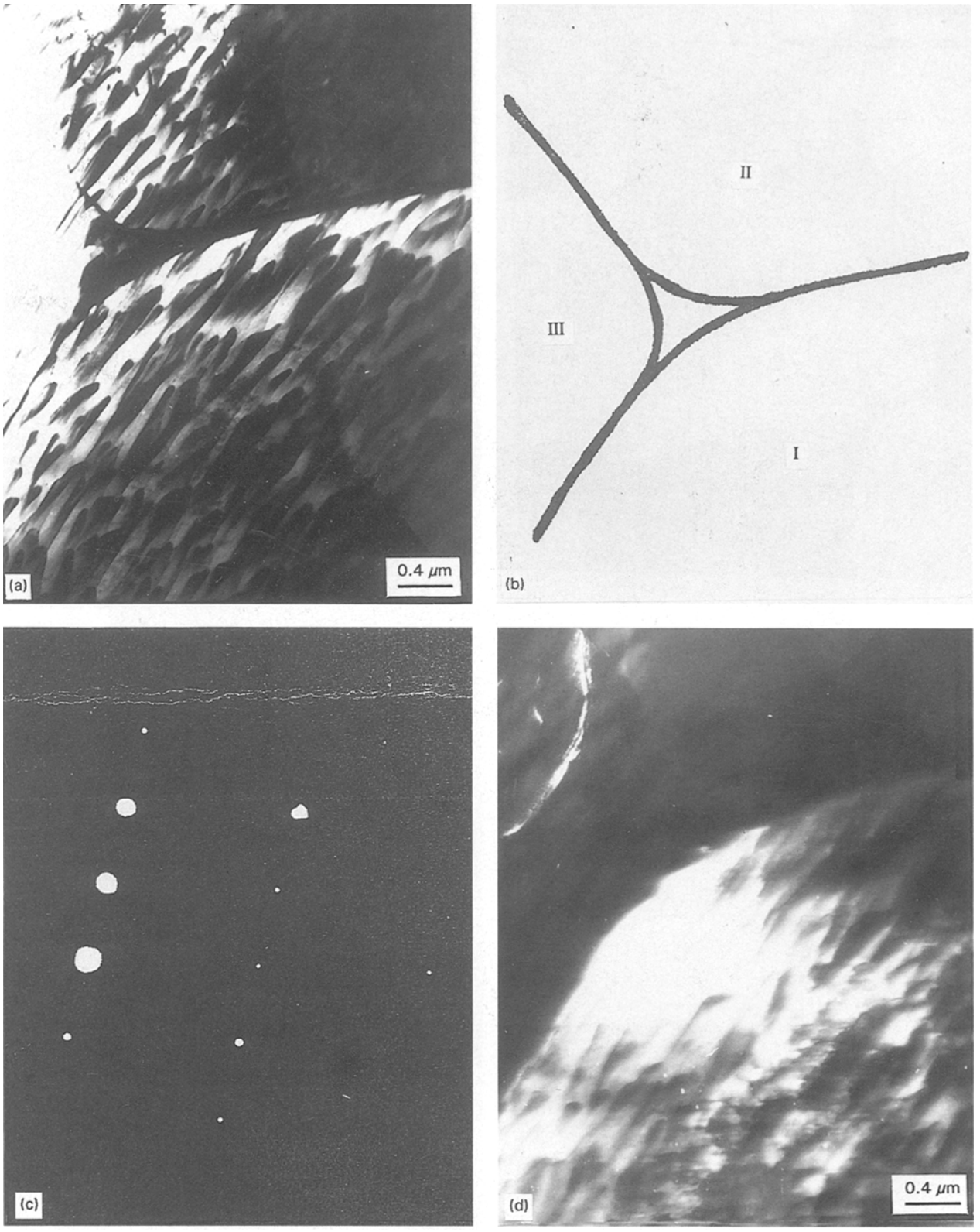

Figure 2 Unique curved grain boundaries in the cold sintered block (a) three grains around a triple junction of grain boundaries, (b) schematic of (a), (c) SAED pattern of grain I, B2 [1 3 3] zone, (d) dark field of grain I ($g = 0\,1\,\bar{1}$).

SEM [10] which indicates that recovery and recrystallization had occurred in the block. This process may not be as complete in comparison with the lower density of dislocations and smaller grains, all with polygon-like morphology, in hot pressed MA NiAl–TiB_2–Y_2O_3 composites [11]. This is probably due to the lower temperature and extensive plastic deformation in the block.

3.2. Metastable phases

Although only a B2 structured β-NiAl phase was identified in the matrix of the cold sintered block by means of XRD [10] a detailed TEM investigation revealed that the block consisted of several kinds of metastable phases. This indicates that the content of the metastable phases is very small and is less than the XRD detected ion limit (about 5 vol %).

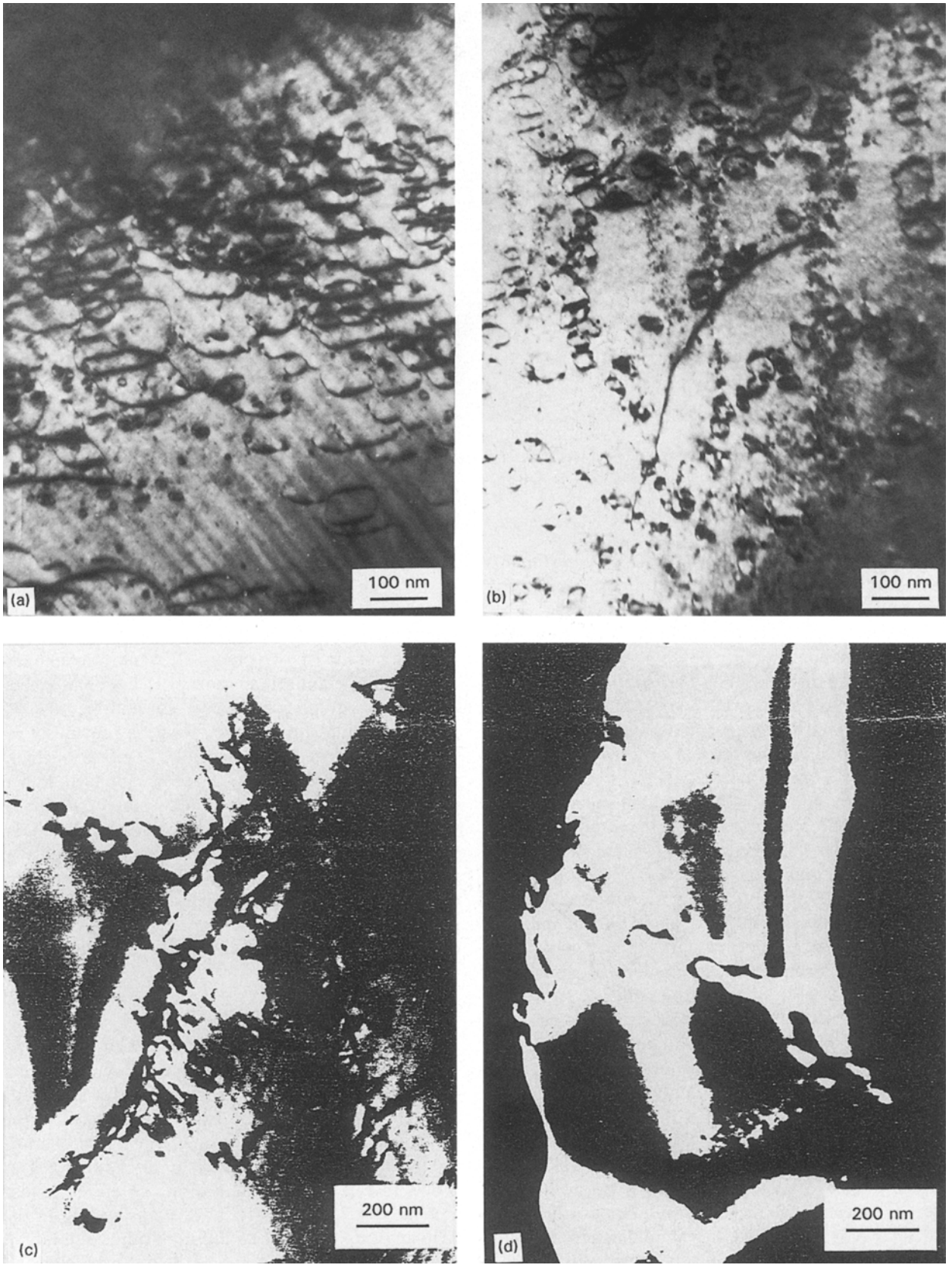

Figure 3 (a) Dislocations in the cold sintered block, (b) high density of dislocations and dislocation loops ($g = 0\bar{1}1$), (c) subgrain boundaries consisting of a dislocation array, (d) dark field of the subgrain boundary ($g = 1\,1\,0$).

3.2.1. Nanocrystalline phase

A nanocrystalline phase (average size 15 nm) is present around ceramic particle agglomerates of TiB_2 and Al_2O_3 is observed on the grain boundaries of some β-NiAl grains as is shown in Fig. 4. Most of the TiB_2 and Al_2O_3 particles in the area show a round or round-like appearance. A few ceramic particles had a special needle-like morphology with a large aspect ratio and contained boron according to EDS examination. This particle is probably TiB which was also

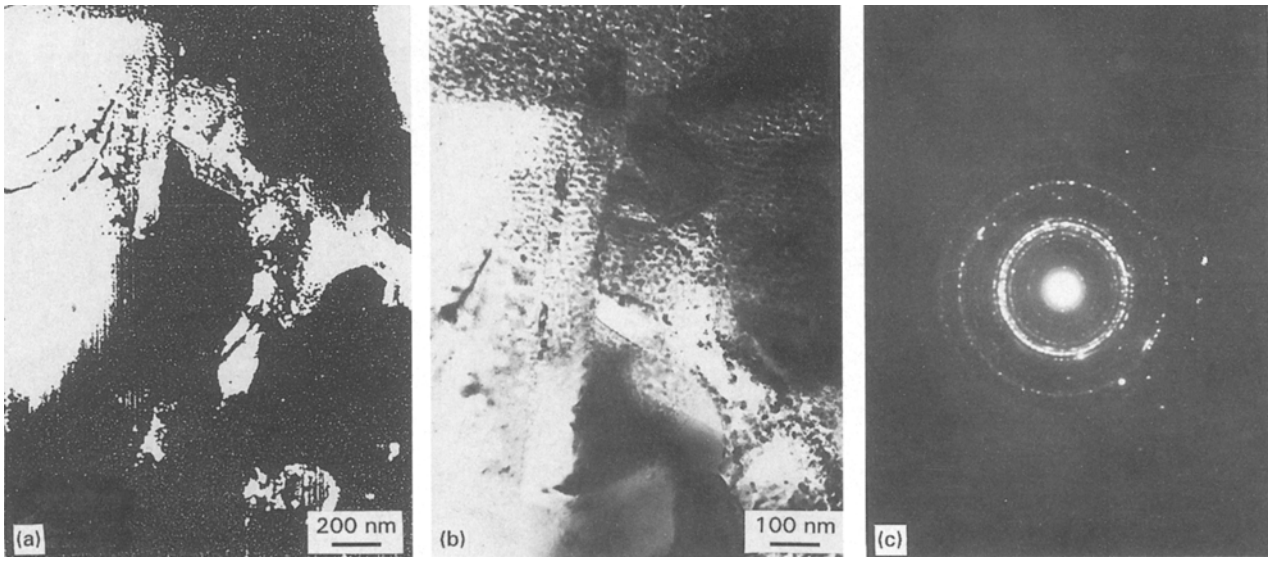

Figure 4 Nanocrystalline phases in the cold sintered block (a) nanocrystalline phases around ceramic particles, (b) larger magnification of (a), (c) SAED pattern of nanocrystalline phases.

found in the MA Ti–B system [16]. It is interesting to note that the nanocrystalline phase almost completely covered the interface of the ceramic particles.

The selected area electron diffraction (SAED) pattern of the nanocrystalline phase consisted of many polycrystalline rings (Fig. 4c). The identification of the pattern based on relevant ASTM cards indicates that the nanocrystalline phase was not a single phase. As is shown in Table II, it contained ordered γ'-Ni_3Al as a major phase and ordered β-NiAl in addition to a γ'-like compound, $Ni_3(AlTi)$, found in a nickel-based superalloy [17]. The diffraction pattern of the $Ni_3(AlTi)$ in the ASTM card [17] is similar to that of γ' but there are additional diffraction peaks due to the partial substitution of titanium for aluminium and consequent lattice distortion. The EDS examination showed that the nanocrystalline phase contained nickel as a main constituent, aluminium, titanium and minor amounts of iron and chromium. The iron and chromium came from the stainless steel balls used in MA and probably together with titanium partially substituted for aluminium to form $Ni_3(AlTiFeCr)$ since the difference in atomic radius between aluminium and iron or chromium is not large. The index corresponding to each diffraction intensity of $Ni_3(AlTi)$ was not given in the ASTM card [17]. It is also impossible for us to do so at this stage due to the error in measuring the accurate composition of $Ni_3(AlTiFeCr)$ using EDS. For simplification, we will not discriminate between the γ'-Ni_3Al and $Ni_3(AlTiFeCr)$ in the remaining part of the present paper. The appearance of the $Ni_3(AlTiFeCr)$ and the possible TiB phase implies that a part of the TiB_2 was dissolved during MA although TiB_2 is quite stable at high temperature.

It is evident that the γ' phase is a metastable phase according to the composition of the cold sintered block in the Ni–Al binary phase diagram [18]. The metastable γ' phase with the nanocrystalline β-NiAl phase were probably formed before the formation of the block in the later stage of MA and the formation of the γ' phase must suppress partially the formation of the stable β-NiAl phase. It is reported that the Gibbs free energy of the B2 structured β-NiAl is lower than that of the $L1_2$ structured Ni_3Al at room temperature in the equilibrium state [19] but that kinetic conditions dominate phase formation in the nonequilibrium state. In fact, we have previously reported [20] that the metastable γ' phase partially replaced the stable β-NiAl phase in rapidly solidified nickel-rich NiAl (average cooling rate $10^6\ K\,s^{-1}$), which is similar to the present situation. Although the specific formation mechanism of the metastable γ' phase in MA and in rapid solidification may be different the local formation of a metastable γ'-Ni_3Al in the nickel-rich (even near-stoichiometric) NiAl or relevant composite is kinetically favourable in nonequilibrium conditions.

3.2.2. Supersaturate solid solution of γ-Ni

A grain in the cold sintered block with curved grain boundaries has been examined by means of SEM [10] and TEM techniques. Of particular interest is the independent triangular area in the junction of three β-NiAl grains all with curved grain boundaries as shown in Fig. 2a. The composition of the triangular area is Ni–8.7 at % Al–1.3 at % Fe according to the EDS analysis. Since the equilibrium solid solubility of aluminium in γ-Ni is about 7 at % [18] the phase in the triangular area should be a metastable supersaturate solid solution of γ-Ni. The preliminary analysis of SAED patterns of the area (Fig. 5) consisted of superimposing it onto a pattern from a β-NiAl grain which indicated that the metastable phase did not possess a f.c.c. structure as does the normal γ-Ni. In addition to that the lattice constant of the phase is quite large. One possibility is that the metastable supersaturate solid solution has a h.c.p. structure since this sort of supersaturate γ-Ni solution was found in the

TABLE II The SAED parameters and identification of nanocrystalline phases*

r_i	3.1	5.1	6.0	7.0	7.8	8.6	9.1	9.8	10.2	11.5	12.3	13.5	14.4	15.2	17.1	17.8	20.5	21.3
I/I_0	W	W	W	W	W	S	VS	M	W	W	W	W	M	M	M	M	W	W
d_i	6.525	3.969	3.370	2.890	2.594	2.352	2.223	2.064	1.983	1.759	1.645	1.533	1.405	1.331	1.183	1.136	0.987	0.950
hkl	?	γ′	γ″	β	γ′	γ″	γ′	β	γ″	γ′	β	γ′	γ′	β	β	γ′	γ′	β
		(100)		(100)	(110)		(111)	(110)		(200)	(111)	(210)	(211)	(210)	(211)	(311)	(222)	(300)

* r_i: radius of ring, I/I_0: relative intensity (W: weak, M: medium, S: strong, VS: very strong), d_i: planar distance, hkl: identified phase or planar index (γ′, γ′-Ni_3Al, γ″: $Ni_3(AlTi)$, β: β-NiAl, ?: cannot be identified).

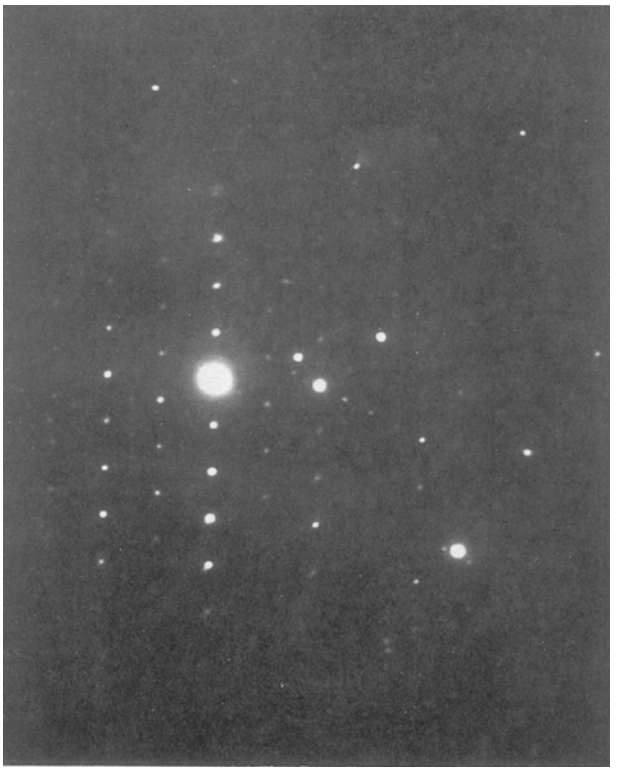

Figure 5 SAED pattern (smaller one) of metastable supersaturate solid solution of γ-Ni in triangular area on junction of grain boundaries (see Fig. 2) superimposed on a bigger pattern of the grain in the area (grain II), B2 [1 1 2] zone.

implantation of antimony into nickel [21] and in the ion irradiation of nickel [22]. The further identification of the crystalline structure of the supersaturate solid solution is in progress.

3.2.3. Amorphous phase

In addition to the metastable crystalline phases, an amorphous phase has also been found in some places of the cold sintered block. Fig. 6a shows an area around the TiB_2 and Al_2O_3 particle agglomerate. The intensive diffuse ring of the SAED pattern of the area in Fig. 6b indicates that the area consisted of an amorphous phase. The unchanged diffuse ring in the SAED pattern and the bright field contrast on repeatedly tilting the foil confirmed this result although the area seems to consist of many very fine particles. The EDS examination showed that the composition of the amorphous phase is close to that of the metastable γ′ phase mentioned above except it contains a little more iron. Similar amorphous phases have been found in MA Ni_3Al [5], MA nickel-rich NiAl [7] and MA NiAlTi [8]. In general a longer time is required to produce an amorphous phase than a nanocrystalline phase in MA [5] thus the present amorphous phase probably resulted from additional milling of the nanocrystalline γ′ phase in the later stage of MA.

Moreover, although many β-NiAl grains in the cold sintered block show the ordered structure (Fig. 1d) some grains of β-NiAl with a metastable disordered structure were also found. For example, the grain below the triangular area (grain I) in Fig. 2 had a disordered B2 structure (Fig. 2c).

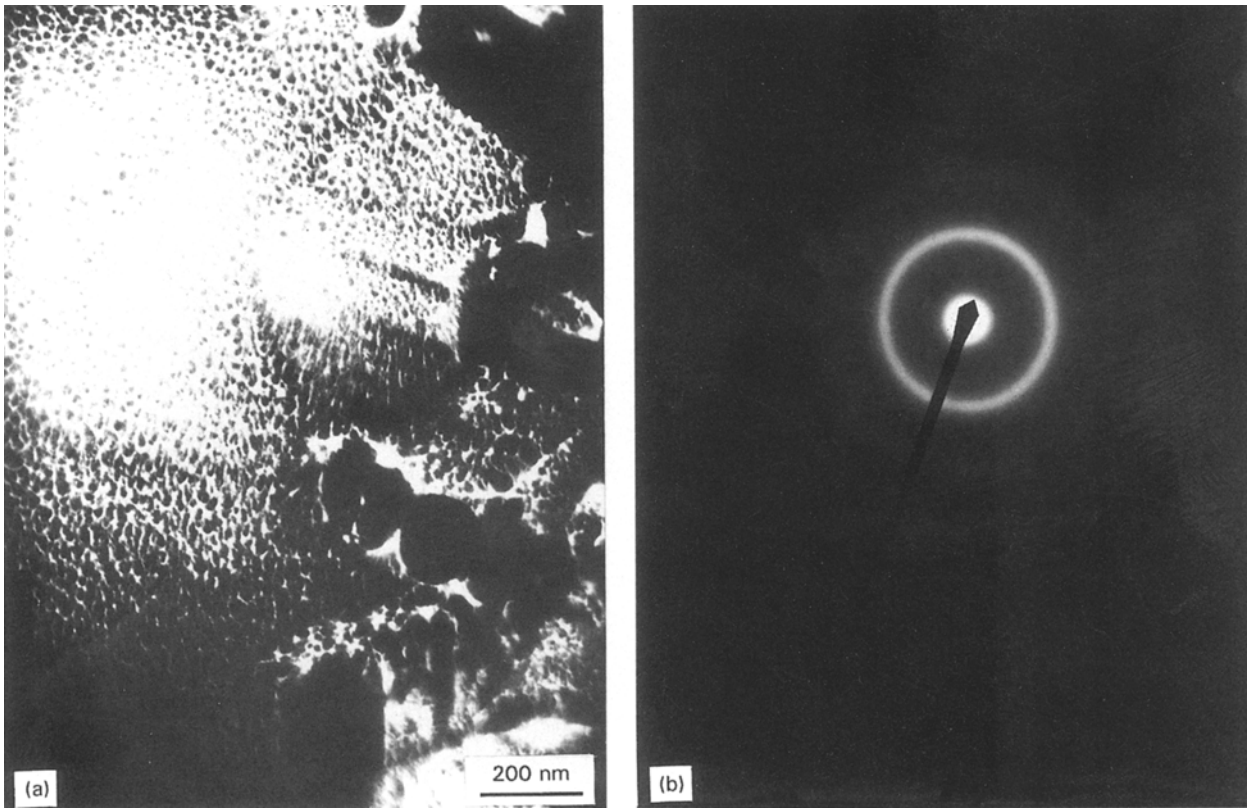

Figure 6 The amorphous phase in the cold sintered block (a) amorphous phase around ceramic particles, (b) SAED pattern of the amorphous phase.

As mentioned previously, B2 structured β-NiAl has a very high negative formation enthalpy and high thermodynamic stability under equilibrium conditions. The competitive formation of the metastable phase in NiAl or NiAl-based composites is possible only when its formation free energy is lower than that of the β-NiAl phase under nonequilibrium conditions. The deformation energy provided by MA is very high, about 5–10 kJ mol^{-1} according to thermal analysis in several CsCl intermetallics [26]. This sort of deformation energy is stored in the MA powders mainly by the formation of defects, grain boundaries and disorder, which certainly raises the formation free energy of the stable β-NiAl phase. Consequently, it is possible that the high density of various defects and local composition distributions in the powders provides the favourable kinetic condition for the formation of metastable phases. However, it is evident from the experimental results in the cold sintered block that the distribution of the metastable phases in the present MA powders is not homogeneous and their content is very limited. This may relate to the previously mentioned stable nature of the β-NiAl and self-heating on MA. Hence, neither relevant diffraction peak was found in the XRD nor patterns of MA powders or the block and the metastable phase was observed in a few MA powders by means of TEM [10]. This is probably why the metastable phase has not been reported in MA NiAl powders before although it also relates closely with processing parameters. Once the MA powders were consolidated by hot pressing or other processing techniques the minor metastable phases must transform into the stable β-NiAl phase. So the cold sintered block produced from the relatively large amount of powders provides a good opportunity to study the minor metastable phases created on MA of NiAl and its composites. It is, of course, also possible that some of the metastable phases in the block transformed into the stable β-NiAl phase due to self-heating on MA.

3.3. The formation mechanism of the cold sintered block

Combined with the SEM and XRD results [10], the above TEM experiments indicate that the microstructure of the cold sintered block is basically similar to that of hot pressed MA NiAl–TiB_2–Y_2O_3, suggesting again that a sintering process occurred at rather low temperatures in the later stage of MA. Due to the relatively low diffusivity in the solid state, heating is important for accelerating diffusion to promote sintering process [23]. These include powder bridging, neck coarsening between powders, releasing gas absorbed by powders, densification and recrystallization. In addition, the higher temperature in normal sintering is also necessary for the reduction of any oxide film on the powders before starting the diffusion between elemental powders. However, the size of the alloyed powders decreases substantially and the grain size reduces down to nanometer scale in the later stage of the MA [10]. The dramatic increase in volume percentage of grain boundaries and vacancy concentration all accelerate the diffusion. The severe collisions in a protective atmosphere during MA provides clean

surfaces amongst the powders and shortens the diffusion distance. All of these factors may help the sintering so that it could proceed partially *in-situ* at lower temperature in the later stage of the MA. Although a vial temperature increase to about 80 °C during MA has been reported [24] this higher temperature is thought to occur locally in the powders during the heavy impacts and thus a local melting assumption during the mechanical grinding of the Co–Y system has been presented to explain the formation of the amorphous phase [25]. Based on the above experimental results, overmilling to a certain extent is one of the conditions to result in the cold sintered block.

In addition, cold sintering in MA must relate closely with powder composition as discussed previously [10], and be associated with the formation of metastable phases according to the present experimental study. According to the distribution of metastable phases in the cold sintered block a mechanism regarding the formation of the block related to its specific composition can be assumed. As seen in Section 3.2.2, the supersaturate γ-Ni was distributed mainly on the junction of curved grain boundaries while the nanocrystalline γ′, including nanocrystalline β, almost completely covered the interface of ceramic particles on the grain boundaries. Considering the good ductility and toughness of γ-Ni solution and the nanocrystalline γ′ [27], (probably including nanocrystalline β), the supersaturate γ-Ni and nanocrystalline γ′ and β may be stuck on and form a "interface adhesive layer" on the surface of some alloyed powders and ceramic particles with larger size in the later stage of MA. When these powders and particles are contacted with each other the ductile layer can combine them together even if they experience extensive impact and friction. The continuation of the process is similar to the growth of a "snow ball" as played by children. The repeated grinding and friction not only promotes a sintering-like densification as discussed above but also makes the block with a flat appearance as observed [10]. Furthermore, due to the small content and inhomogeneous distribution of the metastable phases only a small part of the powders formed the cold sintered block on MA.

Fig. 7 shows additional evidence to support the assumption. In the two sides of a TiB_2 particle on the grain boundaries of a β-NiAl grain there is a metastable γ′ phase, the composition of which is very close to that of the nanocrystalline γ′ phase. Although the grain size of the γ′ phase is larger than a nanometer. Figs. 7(b, c) reveal the fine layer structure in dark field and corresponding streaks in the SAED pattern. Consequently, the TiB_2 particle was probably inhomogeneously covered by many layers of the nanocrystalline γ′ phase before it was combined with other β-NiAl powders to form or to add to the block. The nanocrystalline γ′ may grow and develop into the layer structure during impacts and friction in MA. The amorphous phase probably played a similar role to other metastable phases since it is also distributed around ceramic particles and the amorphous phase normally has good toughness. Additional experiments are necessary to check the supposed formation mechanism of the cold sintered block.

4. Conclusions

(i) The cold sintered block in MA of NiAl–TiB_2 consisted of β-NiAl with a B2 ordered structure TiB_2, and Al_2O_3 particles and also several metastable phases. The coarse Al_2O_3 and some TiB_2 particles are distributed on the grain boundaries of the β-NiAl matrix and many fine TiB_2 particles are within grains. The microstructure of the cold sintered block is similar to that of the hot pressed MA NiAl–TiB_2–Y_2O_3 composite, suggesting that a sintering process occurred *in-situ* at low temperature in the later stage of the MA to form the block.

(ii) A high density of dislocations, including dislocation loops, are present in the cold sintered block, which may relate to extensive plastic deformation during MA and high vacancy concentration in the

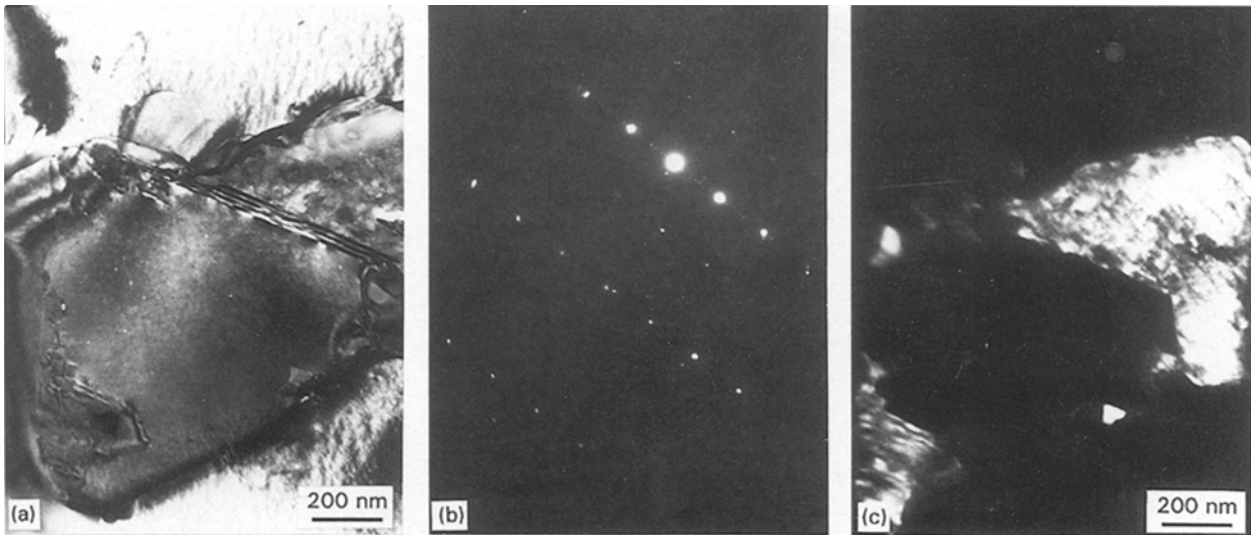

Figure 7 Metastable γ′ phase with a layer structure (a) γ′ phase on two sides of a TiB_2 (T) particle, (b) SAED pattern of γ′ phase, $L1_2$ [1 2 3] zone, (c) dark field of γ′ phase in (a), g = 1 1 1.

MA powders. The high density of dislocations and extensive reaction between dislocations and ceramic particles can explain the good toughness and microhardness of the block. Some subgrain boundaries consisted of dislocation array and polygon-like grain boundaries suggesting that recovery and recrystallization occurred in the cold sintered block.

(iii) Unique curved grain boundaries were found in the cold sintered block existing around the triple junction of grain boundaries and containing an independent triangular area. The grain boundaries are not coherent boundaries and the angle between the boundaries is not small.

(iv) Metastable crystalline phases and an amorphous phase were found in the cold sintered block. The metastable crystalline phases include nanocrystalline or layer-like γ'-Ni_3Al or $Ni_3(AlTiFeCr)$, a supersaturate solid solution of γ-Ni and a disordered β-NiAl phase.

(v) The supersaturate solid solution of γ-Ni with about 3 at% supersolubility contained aluminium and iron distributed on the junction of the curved grain boundaries of β-NiAl grains. A preliminary study indicated that the supersaturate solution does not possess an f.c.c. structure and has a large lattice constant. The composition of the amorphous phase is very close to that of nanocrystalline $Ni_3(AlTiFeCr)$ phase and it is distributed around ceramic particles on grain boundaries. In addition to overmilling to a certain extent, a formation mechanism of the cold sintered block during MA NiAl–TiB_2 relating to the metastable phases has been proposed.

References

1. J. D. WHITTENBERGER, in "Structural Intermetallics" (edited by R. Darolia, J. J. Lewandowski, C. T. Liu, P. L. Martin, D. B. Miracle and M. V. Nathal, TMS, Warrendale, 1993) p. 819.
2. L. WANG, N. BECK and R. J. ARSENAULT, *Mater. Sci. Eng.* **A177** (1994) 83.
3. T. TAKAHASHI and D. C. DUNAND, *ibid.* **A192/193** (1995) 186.
4. TIANYI CHENG, *Scripta Metall. Mater.* **34** (1996) 1377.
5. J. S. C. JANG and C. C. KOCH, *J. Mater. Sci. Res.* **5** (1990) 496.
6. M. D. BARO, S. SURINACH, J. MALAGELADA, M. T. CLAVAGUERA-MORA, S. GIALANELLA and R. W. CAHN, *Acta Metall. Mater.* **41** (1993) 1065.
7. E. IVANOV, T. GRIGORIEVA, V. BOLDYREV, A. B. FASMAN, S. D. MIKHAILENKO and O. T. KALININA, *Mater. Lett.* **7** (1988) 51.
8. M. UMEMOTO, T. ITSUKAICHI, J. CABANAS-MORENO and I. OKANE, in "Proc. 2nd Inter. Conf. on Mechanical Alloying for Structural Application" (edited by J. J. deBarbadillo, F. H. Froes and R. Schwarz, ASM, Materials Park, OH, 1993) p. 245.
9. R. D. NOEBE, R. R. BOWMAN and M. V. NATHAL, *Inter. Mater. Rev.* **38** (1993) 193.
10. TIANYI CHENG, *Scripta Metall. Mater.* **31** (1994) 1599.
11. TIANYI CHENG and M. McLEAN, *Mater. Lett.* **24** (1995) 377.
12. R. DAROLIA, JOM, **3** (1991) 44
13. P. Y. BUTYAGLN, in "Proc. 2nd Inter. Conf. on Mechanical Alloying for Structural Application" (edited by J. J. deBarbadillo, F. H. Froes and R. Schwarz, ASM, Materials Park, OH, 1993) p. 385.
14. D. HULL, " Introduction to Dislocation" (Pergamon, Oxford, 1975) p. 16.
15. J. FRIENDEL, "Dislocations" (Pergamon, Oxford, 1964) p. 93.
16. T. TAKAHASHI, in "Proc. 2nd. Inter. Conf. on Mechanical Alloying for Structural Application" (edited by J. J. deBarbadillo, F. H. Froes and R. Schwarz, ASM, Materials Park, OH, 1993) p. 307.
17. KAUFMAN and PALTO, *Trans. AIME* **218** (1960) 107.
18. T. B. MASSALAKI, Binary Phase Diagrams (ASM, Materials Park, OH, 1986) p. 141.
19. H. ESAKI and M. TOKIZANE, *Mater. Sci. For.* **88–90** (1992) 626.
20. TIANYI CHENG and SHOUHUA ZHANG, *J. Mater. Sci. Lett.* **9** (1990) 953.
21. E. JOHNSON, L. SARHOLT-KRISTENSEN and A. JOHANSEN, *Nucl. Instrum. Methods* **209/210** (1983) 289.
22. V. N. BYKOV, V. A. TROYAN, G. G. ZDOROVTSEVA and V. S. KHAIMOVICH, *Phys. Status Solidi* **A32** (1975) 53.
23. G. C. KUCZYNSKI, "Sintering and Related Phenomena" (Gordon and Breach, New York, 1967).
24. C. KUHRT, H. SCHROPT, L. SCHULTZ and E. ARZTZ, in "Proc. 2nd Inter. Conf. on Mechanical Alloying for Structural Application" (edited by J. J. deBarbadillo, F. H. Froes and R. Schwarz, ASM, Materials Park, OH, 1993) p. 269.
25. A. E. ERMAKOV, E. E. YURCHIKOV and V. A. BOURINOV, *Phys. Met. Metall.* **52** (1981) 50.
26. E. HELLSTERN, H. J. FECHT, Z. FU and W. L. JOHNSON, *J. Mater. Res.* **4** (1989) 1292.
27. G. B. SCHAFFER and A. J. HERON, in "Proc. 2nd Inter. Conf. on Mechanical Alloying for Structural Application" (edited by J. J. deBarbadillo, F. H. Froes and R. Schwarz, ASM, Materials Park, OH, 1993) p. 197.

Received 11 October 1995
and accepted 20 November 1995